

## Cations in Human Rhinoviruses

RUI ZHAO, ANDREA T. HADFIELD,<sup>1</sup> MARCIA J. KREMER, and MICHAEL G. ROSSMANN<sup>2</sup>

*Department of Biological Sciences, Purdue University, West Lafayette, Indiana 47907-1392*

*Received May 30, 1996; returned to author for revision July 16, 1996; accepted October 21, 1996*

All known crystal structures of rhinoviruses have some uninterpreted electron density on their fivefold axes at a distance of about  $152 \pm 3$  Å from the viral center. This density had been assumed to be a  $\text{Ca}^{2+}$  ion, based on its shape, height, and the presence of  $\text{Ca}^{2+}$  ions in the crystallization solutions. Difference electron density maps between EGTA-soaked crystals of human rhinovirus 14 (HRV14), as well as HRV16, and their corresponding native structures show that this density is an EGTA-chelatable ion. Analysis of the coordination geometry indicates that the ions in HRV3, HRV14, and HRV1A could be  $\text{Ca}^{2+}$  and the ion in HRV16 might be  $\text{Zn}^{2+}$ . These cations may play a role in regulation of rhinovirus stability, although the loss of the ion itself does not seem sufficient to lead to viral disassembly. © 1997 Academic Press

### INTRODUCTION

Human rhinoviruses (HRV<sup>3</sup>) belong to the picornavirus family and are a major causative agent of common colds. There are over 100 different serotypes of HRVs, which are divided into at least two groups based on their cellular receptors (Uncapher *et al.*, 1991). The majority of HRVs (belonging to the "major receptor group") use ICAM-1 as their receptor (Greve *et al.*, 1989; Staunton *et al.*, 1989). The remaining rhinoviruses (belonging to the "minor receptor group"), except for HRV87 (Uncapher *et al.*, 1991), utilize the low density lipoprotein receptor (Hofer *et al.*, 1994).

HRVs have pseudo  $T = 3$  icosahedral symmetry. The diameter of the virus is about 300 Å and the molecular weight of the virus is approximately  $8.5 \times 10^6$  Da, including RNA. The viral genome is a (+) RNA strand, which is about 7.2 kb in length. The viral capsid is made of 60 copies of viral proteins VP1 to VP4. VP1, VP2, and VP3 each has a molecular weight of about 30 kDa while VP4 is a 7-kDa small protein which lines the internal surface of the capsid. The crystal structures of HRV14 (Rossmann *et al.*, 1985), HRV16 (Oliveira *et al.*, 1993), and HRV3 (Zhao *et al.*, 1996), all major receptor group viruses, have been

determined, as well as the structure of HRV1A (Kim *et al.*, 1989), a minor receptor group virus. Each of the viral proteins VP1, VP2, and VP3 is folded into an eight-stranded, antiparallel,  $\beta$ -barrel motif whose topology is well conserved in all picornaviruses. The narrow end of the wedge-shaped barrel points toward the icosahedral fivefold axes in the case of VP1, or the quasi-sixfold axes in the case of VP2 and VP3 (Fig. 1).

Human rhinoviruses attach to receptor molecules on the cell membrane and enter the host cell to deliver its RNA by a poorly understood process involving the loss of VP4 and the formation of 125S "A" ("Altered") particles (Lonberg-Holm and Korant, 1972). In polioviruses, the N-terminus of VP1 is externalized and is available for proteolytic cleavage (DeSana and Mandell, 1977). After the "A" particles have released their RNA, they form empty 80S particles. The viral RNA directs the synthesis of a polyprotein, which is subsequently cleaved to form capsid proteins and other nonstructural proteins. In addition, the (+) RNA strand is transcribed into a (–) RNA strand, which subsequently generates new (+) RNA strands for translation and packaging. When the viral proteins have reached sufficient concentration, they assemble into RNA-containing particles. The assembled virion must be stable enough to be able to transfer from one host cell to another, and yet be able to disassemble and release its genome on reinfecting the next cell.

In all of the rhinoviruses for which the structure is known, there is some density on the fivefold axes that cannot be interpreted as a part of the capsid protein. (Although, for convenience, the discussion here is with respect to one specific fivefold, it is equally applicable to all the symmetry-related fivefold axes in the icosahedron). This density has been assumed to be a  $\text{Ca}^{2+}$  ion based on its shape, height, the presence of  $\text{Ca}^{2+}$  ions in

<sup>1</sup> Present address: Rosenstiel Basic Medical Sciences Research Center, Structural Biology Laboratory, Brandeis University, Waltham, MA 02254-9110.

<sup>2</sup> To whom correspondence and reprint requests should be addressed.

<sup>3</sup> Abbreviations used: "A," "Altered"; CHESS, Cornell High Energy Synchrotron Source; EDTA, ethylenediaminetetracetic acid; EGTA, ethylene glycol-bis( $\beta$ -aminoethylether)- $N,N'$ -tetraacetic acid; HRV, human rhinovirus; ICAM-1, intercellular adhesion molecule-1; PEG, polyethylene glycol; STNV, satellite tobacco necrosis virus; SBMV, southern bean mosaic virus; TBSV, tomato bushy stunt virus; VP, viral protein.

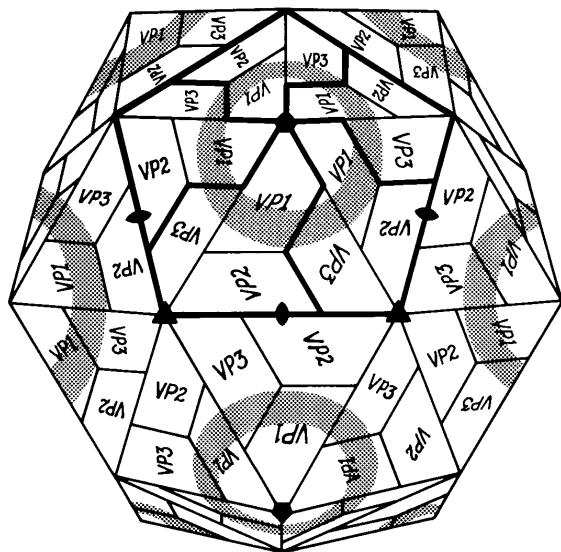


FIG. 1. Diagrammatic view of the pseudo  $T = 3$  icosahedral lattice of human rhinoviruses, showing the position of the viral proteins VP1, VP2, and VP3. The shaded areas are the canyons, the site of receptor attachment.

the crystallization solution and the existence of similar ions in the small icosahedral RNA SBMV (Abdel-Meguid *et al.*, 1981), TBSV (Robinson and Harrison, 1982; Hogle *et al.*, 1983), and STNV (Montelius *et al.*, 1990). The ions in these plant viruses have been demonstrated to be EDTA-chelatable. In TBSV, the ion was replaceable by  $Gd^{3+}$  and, in the case of SBMV, it was proven to be

$Ca^{2+}$  by atomic absorption spectroscopy. Besides these icosahedral plant viruses, putative  $Ca^{2+}$  ions have been observed in the helical tobacco mosaic virus (Pattanayek *et al.*, 1992), the picornavirus coxsackievirus B3 (Muckelbauer *et al.*, 1995), and the ssDNA bacteriophage  $\phi X174$  (Ilag *et al.*, 1994).

The putative  $Ca^{2+}$  ions in HRVs have been proposed to play a role in viral stability (Giranda *et al.*, 1992; Oliveira *et al.*, 1993). When viruses enter the cell, the lower pH of the endosome and the lower  $Ca^{2+}$  concentration in cytoplasm may help to release the  $Ca^{2+}$  ion and facilitate virus uncoating (Durham, 1977, 1978). In this paper, difference electron density maps between EGTA-soaked HRV14, as well as EGTA-soaked HRV16, crystals, and their corresponding native virus crystals are presented, and the identification and possible function of these ions are discussed.

## MATERIALS AND METHODS

### EGTA soaking

EGTA was dissolved to reach a concentration of 1 mM in a buffer (4% PEG 8000 and 10 mM Tris buffer at pH 7.2) suitable for stabilizing HRV14 crystals. HRV14 crystals were grown as described by Rossmann *et al.* (1985) and soaked in the above solution for at least 24 hr before data collection. Concentrations higher than 1 mM EGTA cracked the crystals.

The HRV16 crystals were grown as described by Ol-

TABLE 1  
Diffraction Data

EGTA-soaked crystals	Resolution (Å)	30.0–25.0	25.0–12.5	12.5–8.3	8.3–6.3	6.3–5.0	5.0–4.2	4.2–3.6	3.6–3.1	3.1–3.0
HRV14	No. reflections	190	1,628	4,428	7,472	11,399	16,378	18,299	19,084	5,569
	Percentage of data	19	24	24	20	19	18	14	11	3
	$R_{\text{merge}}^a$	8.9	9.2	8.2	10.0	11.4	12.7	16.3	18.8	25.5
HRV16	No. reflections	94	1,125	3,497	6,247	10,040	15,356	18,911	20,288	6,169
	Percentage of data	7	11	13	12	12	12	11	8	2
	$R_{\text{merge}}^a$	9.2	11.7	9.0	9.7	9.3	9.3	11.7	12.6	15.8
					HRV14			HRV16		
Number of imaging plates					10			17		
Number of crystals					4			4		
Cut-off criteria					$I_h > 5\sigma(I_h)$			$I_h > 3\sigma(I_h)$		
Number of measurements					92,933			90,990		
Number of unique reflections					84,447			81,736		
Overall completeness					14.8			10.0		
Overall $R_{\text{merge}}$					13.6			10.7		
Postrefined effective mosaic spread range										
Vertical					0.05–0.08			0.13–0.16		
Horizontal					0.08–0.12			0.12–0.15		

<sup>a</sup>  $R_{\text{merge}} = [\sum_h \sum_i | \langle I_h \rangle - I_{hi} | / \sum_h \sum_i I_{hi}] \times 100$ , in which  $I_{hi}$  is the  $i$ th measurement and  $\langle I_h \rangle$  is the average intensity of reflection  $h$ .

TABLE 2  
Comparison of EGTA-Soaked Crystals with Native Crystal Data after Local Scaling

EGTA-soaked crystals	Resolution (Å)	30.0–9.0	9.0–6.3	6.3–5.2	5.2–4.5	4.5–4.0	4.0–3.7	3.7–3.4	3.4–3.2	3.2–3.0
HRV14	No. reflections	5,028	8,089	9,466	11,294	11,285	10,681	10,218	9,278	7,172
	Percentage of data	24	20	20	19	16	17	12	12	7
	$R_{\text{diff}}^a$	15.2	13.4	14.1	13.9	15.8	18.8	20.9	23.4	30.5
HRV16	No. reflections	2,608	4,794	6,095	7,139	7,565	7,798	7,048		
	Percentage of data	9	8	9	8	7	9	6		
	$R_{\text{diff}}^a$	14.2	12.2	12.9	13.2	14.3	15.6	17.1		

$$^a R_{\text{diff}} = [\sum_h |F_{\text{EGTA}} - F_{\text{native}}| / \sum_h F_{\text{native}}] \times 100.$$

iveira *et al.* (1993). The EGTA was dissolved in the stabilization buffer for HRV16 crystals (10% PEG 8000 in 0.25 M HEPES/0.25 M NaCl/pH 7.4) and was used to soak HRV16 crystals for at least 24 hr before data collection. Unlike HRV14, the HRV16 crystals were soaked in 100 mM EGTA without cracking.

### Data collection

All of the diffraction data were collected at the CHESS F1 station with an X-ray wavelength of approximately 0.910 Å. The diffraction data were recorded on imaging plates, and these plates were scanned with a Fuji BAS2000 scanner using a 100- $\mu\text{m}$  raster. Both the EGTA-soaked HRV14 and the EGTA-soaked HRV16 crystals diffracted to a resolution of at least 3.0 Å. The crystal-to-plate distances were 300 and 250 mm for HRV14 and HRV16, respectively, and the oscillation angle was chosen to be 0.3° for both HRV14 and HRV16 crystals.

### Data processing and map calculation

The diffraction data for both EGTA-soaked HRV14 and HRV16 crystals were indexed with Kim's auto-indexing program (1989) and then processed and postrefined (Rossmann, 1979; Rossmann *et al.*, 1979).

The EGTA-soaked HRV14 crystals had cell dimensions ( $a = 445.4$  Å with space group  $P2_13$ ) that were very close to those of the native crystals (Rossmann *et al.*, 1985), as far as could be ascertained given the uncertainty of the wavelength of the selected synchrotron radiation. There are two possible orientations of the coordinate system in space group  $P2_13$  related by a fourfold rotation. After each imaging plate was indexed, it was processed both ways. Indexing consistent with the native data was determined by scaling to a small native HRV14 data set. The statistics for the final postrefined data are shown in Table 1. This data set (between 30 and 3.0 Å resolution) was scaled independently within each of 45 resolution shells to the native HRV14 data (Table 2).

The EGTA-soaked HRV16 crystals had cell dimensions ( $a = 362.7$ ,  $b = 347.4$ , and  $c = 335.5$  Å with space group

$P22_12_1$ ) that were close to those of the native crystals (Oliveira *et al.*, 1993). Diffraction data from 14 imaging plates were processed and postrefined. The statistics of the postrefined data are shown in Table 1. This data set (between 30 and 3.4 Å resolution) was scaled independently within each of 35 resolution shells to the native HRV16 data (Table 2).

Difference maps between the EGTA-soaked crystals and the native crystals were calculated using the Fourier coefficients  $(F_D - F_N)\omega_N \exp(i\alpha_N)$  (Smith *et al.*, 1986), where  $F_D$  and  $F_N$  are the structure factor amplitudes of the EGTA-soaked virus crystals and of the native virus crystals, respectively,  $\alpha_N$  is the native phase obtained from the molecular replacement and real-space averaging procedure and  $\omega_N$  is a weighting factor dependent on the consistency between the  $F_N(\text{obs})$  and  $F_N(\text{calc})$  obtained from the Fourier back-transformation of the averaged native map. All available matched data to 3.5 Å resolution were included. The resultant difference maps were then averaged using the 20- and 30-fold noncrystallographic redundancy in HRV14 and HRV16, respectively (Rossmann *et al.*, 1992). The averaged maps were suitably oriented with icosahedral axes parallel to a selected orthogonal grid. The maps were viewed with the program O (Jones *et al.*, 1991).

## RESULTS

The difference map between the EGTA-soaked and native HRV14 electron density shows a negative peak on the viral fivefold axis (Fig. 2a) at the position of the putative  $\text{Ca}^{2+}$  ion and also a negative peak on the threefold axis (Fig. 2b). The latter corresponds to positive electron density in the native map that had been interpreted as a water molecule.

The native HRV14 structure, solved in 1985, had a leucine at residue 2170.<sup>4</sup> However, this residue had spontaneously mutated to a valine residue in HRV14 which had

<sup>4</sup> Residues in each viral protein are numbered sequentially starting at 1001, 2001, 3001, and 4001 for VP1, VP2, VP3, and VP4, respectively.

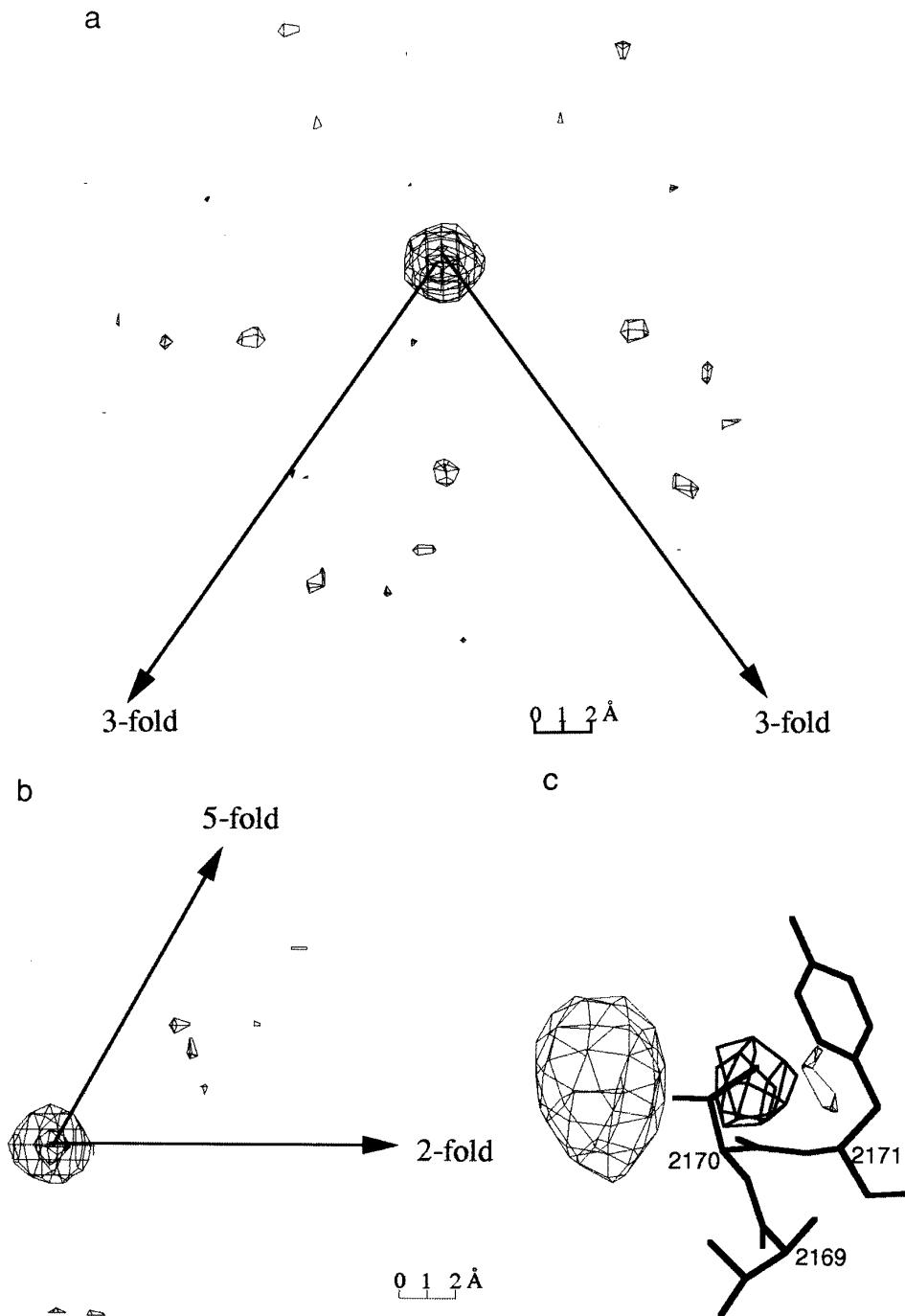


FIG. 2. (a) The negative density on the fivefold axis in the [(EGTA-soaked HRV14) – (HRV14)] difference map. The density is contoured at an approximately  $1\sigma$  level. Positive contours are omitted. The orientation of this figure is looking down the fivefold axis. The lines radiate from the fivefold axis and point toward the nearest threefold axes. (b) The negative density on the threefold axis in the [(EGTA-soaked HRV14) – (HRV14)] difference map. The density is contoured at an approximately  $1\sigma$  level. Positive contours are omitted. The orientation of this figure is looking down the threefold axis. The lines radiate from the threefold axis and point toward the nearest fivefold axis and twofold axis. (c) Positive (thick lines) and negative (thin lines) densities around residue 2170 (a valine in the soaked crystals and a leucine in the native virus) in the [(EGTA-soaked HRV14) – (HRV14)] difference map. The density is contoured at an approximately  $1\sigma$  level.

been grown since 1985 (Smith *et al.*, 1986). The difference map between the EGTA-soaked HRV14 and the native HRV14 shows negative density corresponding to this mutation (Fig. 2c), which can serve as a control. The

densities mentioned above are at least two times larger than any other peaks on the map.

The difference map between the EGTA-soaked and native HRV16 electron density shows a negative peak,

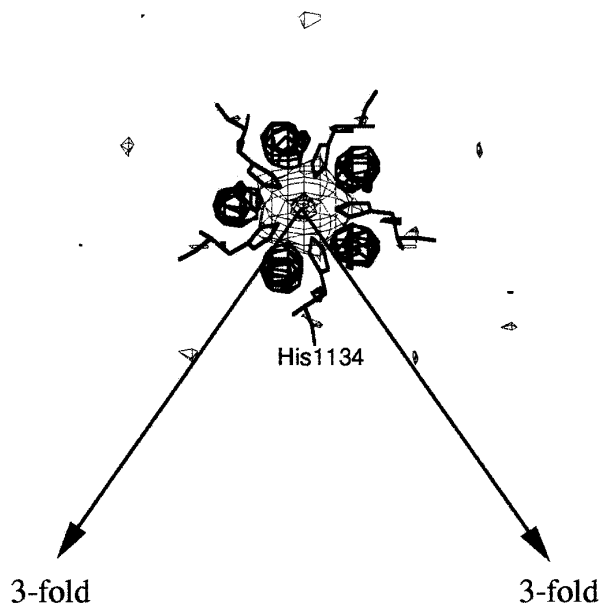


FIG. 3. Positive (thick lines) and negative (thin lines) density around the fivefold axis in the [(EGTA-soaked HRV16) – (HRV16)] difference map. The density is contoured at an approximately  $0.75\sigma$  level. The orientation of this figure is looking down the fivefold axis. The lines radiate from the fivefold axis and point toward the nearest threefold axes.

four times bigger than any other peaks on the map, on the viral fivefold axis and some smaller positive peaks surrounding this negative peak (Fig. 3). These positive peaks could be Fourier “ripples” caused by truncation of the Fourier synthesis. The discontinuity in the spherical “ripples” might be due to the ligand interaction with the metal ion.

The above results show that the density on HRV14 and HRV16 fivefold axes and the density on HRV14 threefold axes correspond to EGTA-chelatable metal ions. Presumably, density at equivalent positions in HRV1A and HRV3 are similar ions.

## DISCUSSION

The icosahedral electron density averaging process has larger error on the icosahedral symmetry axes, as these special positions have a lower order of noncrystallographic redundancy. This is especially true on the fivefold axes. Thus, interpretation of high or low density peaks along these axes must be done with caution. However, the repeated occurrence of these peaks at chemically equivalent positions on numerous different data sets in a number of different HRV serotypes, as well as in a coxsackievirus B (Muckelbauer *et al.*, 1995), drew attention to the presence of a possible ion on the fivefold axes. Had these peaks been the effect of random error, they would have occurred at any position along the symmetry axes, not just at certain fixed positions. Further-

more, the electron density occurred at a site that was chemically ideal for cation binding in all these homologous viruses. The EGTA experiments described here, which cause major changes of the density at this site while not disturbing other features in the electron density map, establish these special sites as cations beyond any reasonable room for doubt.

Knowledge of the amino acid sequence of the capsid proteins and the excellent electron density always present in the structure determination of icosahedral viruses leaves no doubt as to the nature of the ligands surrounding the cation sites. However, their accurate positioning will depend on the resolution and quality of the data. The results given here establish the site and nature of the cation binding sites for the structures of HRV14 (2.4 Å resolution), HRV3 (3.0 Å resolution), HRV16 (2.15 Å resolution), and HRV1A (3.2 Å resolution). The site of the ion on a symmetry axis constrains the averaged position of the ligands, although the ligands might not adhere to precise icosahedral fivefold symmetry. The exact distances from the ligands to the ion are, therefore, rather approximate and although less than 0.5 Å in error. However, the number and type of the ligands are clear.

## Coordination geometry of the metal ion in rhinoviruses

In HRV14 (refined to 2.4 Å resolution; B. Berger and M. G. Rossmann, unpublished results), the metal ion located on the fivefold axis is approximately 155 Å from the viral center. This ion coordinates with the main chain carbonyl oxygen atom from each of the five symmetry-related Asn1141 residues. The ion appears to be in the plane formed by the five carbonyl oxygen atoms. The ion-ligand distance is 2.7 Å. There is one water molecule on the viral fivefold axis above (above indicates a direction toward the exterior of the virus) the metal ion at a distance of 2.6 Å away from the ion. Another water molecule on the viral fivefold axis is below the metal ion at a distance of 2.9 Å. The ion, thus, forms a pentagonal bipyramid with seven ligands (Fig. 4). The electron density height of the ion is roughly 80% of the protein backbone densities. The water molecules above and below the ion are approximately 75 and 50% of the height of the protein backbone density, respectively (Table 3).

The metal ion on the threefold axis of HRV14 is approximately 151 Å away from the viral center, and it coordinates with the side chain  $O_{\epsilon 1}$  atom from each of the three symmetry-related Glu3200 residues. The ion is approximately 1.2 Å above the plane formed by the three symmetry-related  $O_{\epsilon 1}$  atoms, and the ion-ligand distance is 2.4 Å. The ion density is roughly the same height as the protein backbone densities. The residues corresponding to Glu3200 in HRV14 are Gln3200, Asn3202, and Ser3202 in HRV3, HRV16, and HRV1A, respectively. The shortest

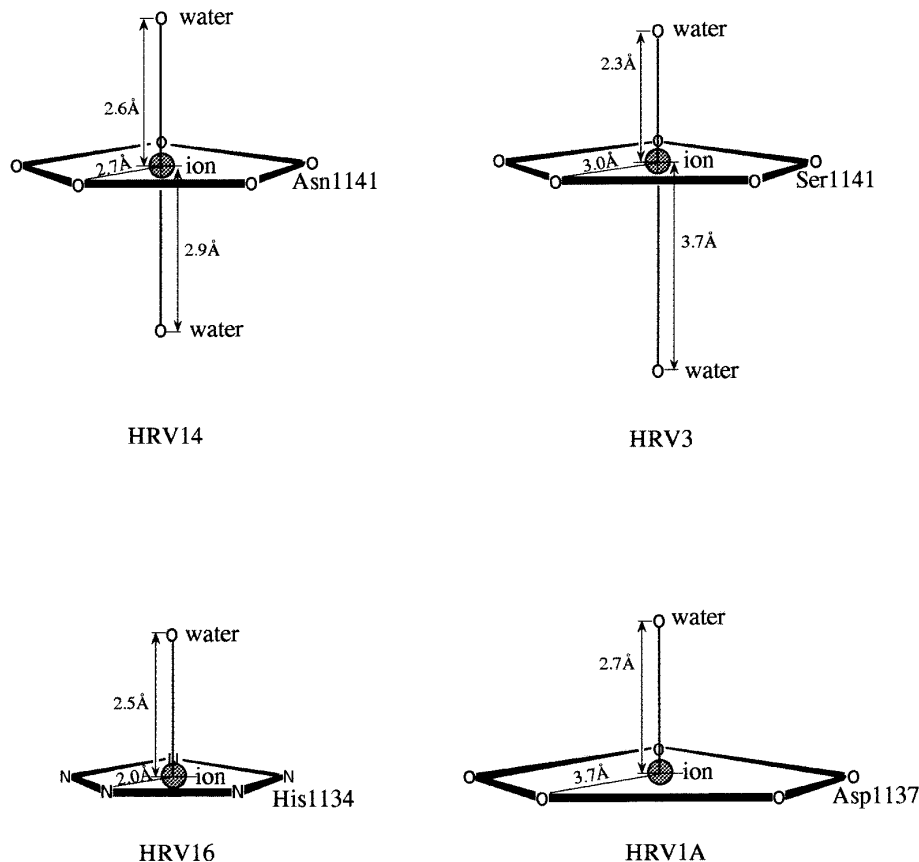


FIG. 4. Diagrammatic representation of the ion ligand coordination on the fivefold axis.

distances from the corresponding atoms to the viral threefold axis are 2.0 Å, 1.8 Å, and 3.2 Å, respectively. Although these atoms have the potential to bind an ion, there is no density at this site on the threefold axes of HRV3, HRV1A, and HRV16 (Table 3).

In HRV3 (unrefined structure at 3.0 Å resolution; Zhao *et al.*, 1996), the ion on the viral fivefold axis is approximately 155 Å away from the viral center, and it also forms a pentagonal bipyramid structure with seven ligands. The ion is roughly in the pentagonal plane formed by five symmetry-related main chain carbonyl oxygens of Ser1141 with an ion-ligand distance of 3.0 Å (Fig. 4). Water molecules are situated on the fivefold axis above and below the metal ion at a distance of 2.3 and 3.7 Å, respectively, very similar to the geometry in HRV14. In HRV3, the density of this metal ion is weaker than its surrounding protein and is only about 60% of the protein backbone density. The densities of the water molecules above and below the ion are roughly 50 and 75% of the protein backbone density, respectively (Table 3).

In HRV16 (refined to 2.2 Å resolution; Hadfield *et al.*, 1996), the metal ion on the viral fivefold axis coordinates with the  $N_{\epsilon 2}$  atom from each of five symmetry-related side chains of His1134. The ion is located at 152 Å from the viral center and is roughly in the pentagonal plane formed

by the symmetry-related  $N_{\epsilon 2}$  atoms. The ion-ligand distance is 2.0 Å (Fig. 4). A water molecule is situated on the viral fivefold axis above the ion at a distance of 2.5 Å. However, no water molecule is visible below the ion. In HRV16, the ion density is about twice as strong as the average protein backbone density, and the density of the water molecule is roughly the same as the surrounding protein densities (Table 3).

The metal ion on the fivefold axis in HRV1A (unrefined structure at 3.3 Å resolution; Kim *et al.*, 1989) is approximately 150 Å away from the viral center and has six ligands. The ion coordinates with the side chain  $O_{\delta 2}$  atom from each of five symmetry-related Asp1137 residues with an ion-ligand distance of 3.7 Å. The ion is approximately in the pentagonal plane formed by the symmetry-related  $O_{\delta 2}$  atoms. There is one water molecule on the fivefold axis at a distance of 2.7 Å above the ion. There is no apparent water molecule below the ion. The densities of both the ion and the water molecule are roughly 90% of the protein backbone densities.

In the structure of another picornavirus, coxsackievirus B3, there are two putative  $Ca^{2+}$  ions or water molecules on the fivefold axes and one  $Ca^{2+}$  ion on the threefold axes (Muckelbauer *et al.*, 1995). The ions (or water molecules) on the fivefold axes are at a distance of 153 and

TABLE 3  
Coordination Geometry of Cations in Rhinoviruses

Viruses	HRV14	HRV3	HRV16	HRV1A	
Ion density height relative to an average protein backbone density height of 1	0.8	0.6	2.0	0.9	
Ion on the fivefold axis	Radial distance (Å)	155	155	152	150
	Number of ligands	7	7	6	6
	Ligand type (distance to the ion)	Carbonyl oxygen of N1141 (2.7 Å)	Carbonyl oxygen of S1141 (3.0 Å)	N <sub>e2</sub> of H1134 (2.0 Å)	O <sub>δ2</sub> of D1137 (3.7 Å)
Water on the fivefold axis above the ion (distance to the ion)	2.6 Å	2.3 Å	2.5 Å	2.7 Å	
Water on the fivefold axis below the ion (distance to the ion)	2.9 Å	3.7 Å	No water	No water	
Ion density height relative to an average protein backbone density height of 1	1.0	No density	No density	No density	
Ion on the threefold axis	Radial distance (Å)	151	—	—	—
	Number of ligands	3	3 <sup>a</sup>	3 <sup>a</sup>	3 <sup>a</sup>
	Ligand type (distance to the ion)	O <sub>e1</sub> of E3200 (2.4 Å)	O <sub>e</sub> or N <sub>e</sub> of Q3200 (2.0 Å)	O <sub>δ</sub> or N <sub>δ</sub> of N3202 (1.8 Å)	O <sub>γ</sub> of S3202 (3.2 Å)

<sup>a</sup> Potential ligands for a bound ion. Shown are the shortest distances from the potential liganding atoms to the viral threefold axis.

147 Å from the viral center. These ions are approximately 60% of the height of the protein backbone electron density and might form water-mediated interactions with the side chain oxygens of the fivefold-related Asp1133 residues and with the main chain oxygens of Gln1132. The ion which is 153 Å away from the viral center corresponds to the ions on the fivefold axes of the rhinoviruses described above. Another putative ion is located on the icosahedral threefold axis of coxsackievirus B3 at approximately 148 Å from the viral center. This ion coordinates with six side chain oxygens of the threefold-related residues of Asp3203, which correspond to the Glu3200 residues that coordinate with an ion on the threefold axes in HRV14. A seventh ligand is a water molecule directly below the ion. The distances between the ion and its protein ligands, as well as between the ion and the water ligand, are all 2.7 Å. The electron density of this ion is approximately twice the height of the surrounding protein atoms.

In type 1, Mahoney strain, poliovirus (Hogle *et al.*, 1985), density on the fivefold axis was assigned to be an anion. This anion is 155 Å from the viral center and would be 2.2 Å away from the N<sub>e2</sub> atoms of His1149, if the imidazole ring were rotated by 180°. His1149 of poliovirus type 1 corresponds to His1134 in HRV16 and Asn1141 in HRV14, residues that have now been assigned as cation ligands. Densities on the threefold axis of type 1 and type 3 (Filman *et al.*, 1989) polioviruses, at a radial distance of 147 Å and 148 Å, respectively, were also assumed to be anions. The ions interact with the O<sub>γ</sub> atoms from three symmetry-related Ser3203 residues and an oxygen from a water molecule on the threefold

axis below the ion. The ion-ligand distances are all 2.5 Å in type 1 and between 3.0 and 3.3 Å in type 3 polioviruses. Residue Ser3203 in poliovirus is equivalent to Glu3200 in HRV14, where it is a ligand for a Ca<sup>2+</sup> ion.

#### Probable identification of metal ions from coordination geometry

Some metal ions commonly seen in biological systems, for example, Ca<sup>2+</sup>, Mg<sup>2+</sup>, Cu<sup>2+</sup>, and Zn<sup>2+</sup>, are EGTA-chelatable. The formation constants (for definition, see Table 4) of EGTA with Cu<sup>2+</sup> and Zn<sup>2+</sup> are higher than those for Ca<sup>2+</sup> and Mg<sup>2+</sup> (Table 4). Thus, it cannot be assumed that the densities on the fivefold or threefold axes of rhinoviruses belong to Ca<sup>2+</sup> ions solely because they are EGTA removable.

TABLE 4  
Formation Constants<sup>a,b</sup> of EGTA for Various Biologically Active Metal Ions

Metal ion	EGTA
Ca <sup>2+</sup>	10.9
Co <sup>2+</sup>	12.3
Cu <sup>2+</sup>	17.8
Mg <sup>2+</sup>	5.4
Mn <sup>2+</sup>	12.3
Zn <sup>2+</sup>	14.5

<sup>a</sup> Taken from Handbook of Analytical Chemistry (Aikens and Reilly, 1963).

<sup>b</sup> Formation constant for an ion-EGTA complex:  $\log \left( \frac{[\text{ion} - \text{EGTA}]}{([\text{ion}] \times [\text{EGTA}])} \right)$ , where [ ] indicates the concentration of a certain sample.

In the structural refinement of proteins, the interatomic distances and angles of putative ions need not be restrained, because they are well separated from the nearest protein atoms. Thus, their coordination distances and geometry can be indicators of the identity of the ion. In  $\text{Ca}^{2+}$  binding proteins, the  $\text{Ca}^{2+}$  ligands are dominantly oxygen atoms (McPhalen *et al.*, 1991). In many proteins,  $\text{Ca}^{2+}$  ions have at least one ligand associated with a main chain carbonyl oxygen.  $\text{Ca}^{2+}$  ions can accommodate 4 to 12 oxygen ligands, but coordination numbers of 6, 7, and 8 are the most common. Six ligands tend to form an octahedron and 7 ligands tend to form a pentagonal bipyramid with 5 atoms in the equatorial plane. A coordination geometry with 5 or 6 ligands displaying a distorted pentagonal bipyramid has also been observed. In proteins, the "missing" ligands are usually presumed to be disordered water molecules (McPhalen *et al.*, 1991). The mean  $\text{Ca}^{2+}$ -ligand distance varies from 2.0 to 3.2 Å, with the average value being about 2.4 Å (McPhalen *et al.*, 1991).

$\text{Zn}^{2+}$  ions are often found in association with the nitrogen atoms of histidine (Glusker, 1991). The coordination number of  $\text{Zn}^{2+}$  is usually four, five, or six. When a  $\text{Zn}^{2+}$  ion has six ligands, they tend to lie on the vertices of an octahedron. The observed  $\text{Zn}^{2+}$ -nitrogen distance is between 2.0 and 2.3 Å, with the average being 2.1 Å (Vedani and Huhta, 1990; Glusker, 1991).

The coordination geometry, ligand type, and ion-ligand distances (Table 3) are consistent with  $\text{Ca}^{2+}$  for the ions on the fivefold axes of HRV14, HRV3, and HRV1A, although the distances in the case of the poorly determined HRV1A structure are rather large. In HRV16, the ion on the fivefold axis (Table 3) has a coordination geometry consistent with a  $\text{Ca}^{2+}$  ion, but the distances are rather short and the ligands are nitrogen atoms. There are no known examples where a  $\text{Ca}^{2+}$  ion is liganded by nitrogen atoms in proteins (McPhalen *et al.*, 1991). However, in a structure determination of inosine 5'-monophosphate (Brown and Bugg, 1980) a  $\text{Ca}^{2+}$  ion is liganded by a nitrogen atom at a distance of 2.7 Å, rather longer than the 2 Å distance found in HRV16. The geometry and ligand type would be consistent with a  $\text{Zn}^{2+}$  ion on the HRV16 fivefold axis. The much larger height of the fivefold, nonprotein peak in HRV16 would also suggest an ion with a larger atomic number, such as  $\text{Zn}^{2+}$  (atomic number of 30) as opposed to  $\text{Ca}^{2+}$  (atomic number of 20). This would explain why the Fourier "ripples" were observed in the EGTA-soaked HRV16 structure but not in the EGTA-soaked HRV14 structure. Thus, while  $\text{Ca}^{2+}$  would be a possible ligand, the weight of evidence is in favor of  $\text{Zn}^{2+}$ , presumably derived from the cytoplasm during assembly.

The coordination of the ion on the threefold axis in HRV14 is consistent with  $\text{Ca}^{2+}$ , but the three observable

ligands are too few compared with a normal  $\text{Ca}^{2+}$  binding environment.

### Probable identification of metal ions from valence calculation

A number of computational algorithms have been developed to predict metal ion binding sites in proteins. The valence calculation method is especially useful (Nayal and Di Cera, 1994) for this purpose, although it is dependent upon the availability of accurate coordination distances. In this method, the potential valence,  $v$ , of a point in the structure is calculated for a specific ion as

$$v = \sum_{j=1}^M \left( \frac{R_j}{R_0} \right)^{-N} \quad (1)$$

$$\text{or } v = \sum_{j=1}^M \exp[(r_o - R_j)/B] \quad (2)$$

where  $R_j$  is the distance between the ion and the  $j$ th ligand in the coordination shell and  $M$  is the total number of ligands surrounding the ion.  $R_0$  and  $N$  (Brown and Wu, 1976), as well as  $r_o$  and  $B$  (Brown and Altermatt, 1985), are empirical parameters associated with a specific ion-ligand pair which translate the bond lengths into bond strengths.

Valences have been calculated for different ions on the fivefold and threefold axes of HRV14, HRV3, and HRV1A (Table 5). HRV16 had to be excluded from these calculations as no empirical values of the constraints in Eqs. (1) or (2) were available for ion-nitrogen pairs. The results show that the cation binding site on the fivefold axis has the highest valence for  $\text{Ca}^{2+}$  among the common biologically active cations, although the valence values for  $\text{Ca}^{2+}$  are much lower than the expected value of 2. In HRV14, each of the seven oxygen atoms would have to move 0.3 Å closer to the ion to reach a valence of 2. In the unrefined HRV3 and HRV1A structures, the low valences could be due to inaccuracies of the ligand and ion positions. The low valences may also reflect weak binding affinity of  $\text{Ca}^{2+}$  to these viruses, as suggested by the low electron density (Table 3).<sup>5</sup>

The electron density representing the putative ions in the icosahedral plant viruses in SBMV, STNV, and TBSV can be removed by soaking crystals in EDTA. The ions in SBMV and TBSV have been suggested to be  $\text{Ca}^{2+}$  ions either from atomic absorption spectroscopy or from the ability of these ions being replaceable by  $\text{Gd}^{2+}$ . There is at least one putative ion binding site in these viruses

<sup>5</sup> The low occupancy of the  $\text{Ca}^{2+}$  ions will result in a mixture of liganded and unliganded states. Where an ion is not bound, the liganding side chains will be further apart. Averaging electron density for the two states would give ligand distances greater than is the case for the liganded state on its own.

TABLE 5a  
Valences for Potential Divalent Cations According to Equation (1)

Cation	HRV14		HRV3 Fivefold	HRV1A Fivefold	SBMV		TBSV Site G1
	Threefold	Fivefold			Site A	Site C	
Ca <sup>2+</sup>	0.87	1.06	0.83	0.29	1.94	1.91	1.82
Co <sup>2+</sup>	0.48	0.57	0.44	0.15	1.07	1.05	1.01
Cu <sup>2+</sup>	0.40	0.46	0.36	0.12	0.94	0.92	0.90
Mg <sup>2+</sup>	0.56	0.78	0.61	0.26	1.15	1.14	1.06
Mn <sup>2+</sup>	0.60	0.71	0.55	0.19	1.34	1.32	1.27
Zn <sup>2+</sup>	0.44	0.49	0.39	0.13	1.02	1.00	0.98

that has a valence close to 2 for Ca<sup>2+</sup> (Table 5). This may reflect a tighter binding of Ca<sup>2+</sup> ions to these viruses compared with those in rhinoviruses. It may also explain the expansion of these plant viruses upon extraction of Ca<sup>2+</sup> ions which is not observed in rhinoviruses. The valence for Ca<sup>2+</sup> at site B is large (~3) in SBMV due to three short ion–ligand distances, possibly as a result of coordinate error. There is considerable variation (from 0.5 to 2.8) in the valence of the putative Ca<sup>2+</sup> binding sites in TBSV. This again is likely to be due to coordinate error. This variation is even larger among the putative Ca<sup>2+</sup> binding sites in STNV.

If an ion were to exist on the threefold axes of HRV3 or HRV16 at the same position as the ion in HRV14, the valence for a Ca<sup>2+</sup> ion would be 1.1 and 1.4, respectively. Thus, HRV3 and HRV16 should have the potential for binding a Ca<sup>2+</sup> ion on their threefold axes, although no density was observed at these positions.

### Possible functions of the metal ion

The results reported here establish that there are metal binding sites on the fivefold axes of the rhino and entero picornaviruses. Although some uncertainty remains about the exact identity of these ions, nevertheless, their dependence on pH (Giranda *et al.*, 1992) and the binding of antiviral compounds (Smith *et al.*, 1986), supported by the presence of similarly positioned ions in other icosahedral vi-

ruses (Muckelbauer *et al.*, 1995), suggest their importance to viral function. The major functions of metal ions in a protein are to enhance stability and to participate in the catalytic processes of enzymes. Metal ions can activate chemical bonds and make them more amenable to reaction. They can also take part in the regulation processes of a protein by altering the protein conformation upon binding. In certain instances, ions can alternate between different oxidation states and help electron transfer. Sometimes a specific ion is needed to perform a particular function, while in other cases a variety of similarly sized ions can perform the same function. Binding of Ca<sup>2+</sup> ions to proteins is frequently associated with increasing stability to various denaturants (McPhalen *et al.*, 1991) or causing major conformational alterations (Concha *et al.*, 1993). Similarly, cations may be regulating virion stability in the assembly and uncoating processes of rhino and other picornaviruses.

Metal ions on the symmetry axes of rhinoviruses, coxsackieviruses B3, and polioviruses may help to stabilize the capsid and regulate viral disassembly (Giranda *et al.*, 1992). In the cytoplasm of a resting cell, the Ca<sup>2+</sup> concentration is normally several orders of magnitude lower than that outside the cell (0.2  $\mu$ M versus 2 mM). When these viruses enter the cell, the lower Ca<sup>2+</sup> concentration in the cytoplasm may lead to loss of bound Ca<sup>2+</sup> and, hence, could lead to viral uncoating and RNA release. The presence of the Ca<sup>2+</sup> can also be controlled by pH variation as was shown to be the case for the ions on the fivefold axes of HRV14 (Giranda *et al.*, 1992). In the case of HRV16, the low pH in endosomes might protonate the nitrogen atoms of the histidine ligands around the fivefold axes, resulting in positively charged imidazole groups, leading to the loss of the putative Zn<sup>2+</sup> ions.

Although the metal ion may play a role in viral disassembly, no conformational changes were observed in the EGTA-soaked HRV14 and HRV16 structures. However, higher concentrations of EGTA caused crystal cracking. Thus, the loss of a limited number of metal ions was not enough to lead to viral disassembly, but could make the virus more susceptible to environmental factors.

The protein structure surrounding the rhinovirus five-

TABLE 5b

Valences for Potential Divalent Cations According to Equation (2)

Cation	HRV14		HRV3 Fivefold	HRV1A Fivefold
	Threefold	Fivefold		
Ca <sup>2+</sup>	0.93	0.95	0.85	0.18
Co <sup>2+</sup>	0.44	0.45	0.40	0.08
Cu <sup>2+</sup>	0.43	0.44	0.39	0.09
Mg <sup>2+</sup>	0.44	0.45	0.41	0.09
Mn <sup>2+</sup>	0.58	0.59	0.53	0.11
Zn <sup>2+</sup>	0.46	0.47	0.42	0.09

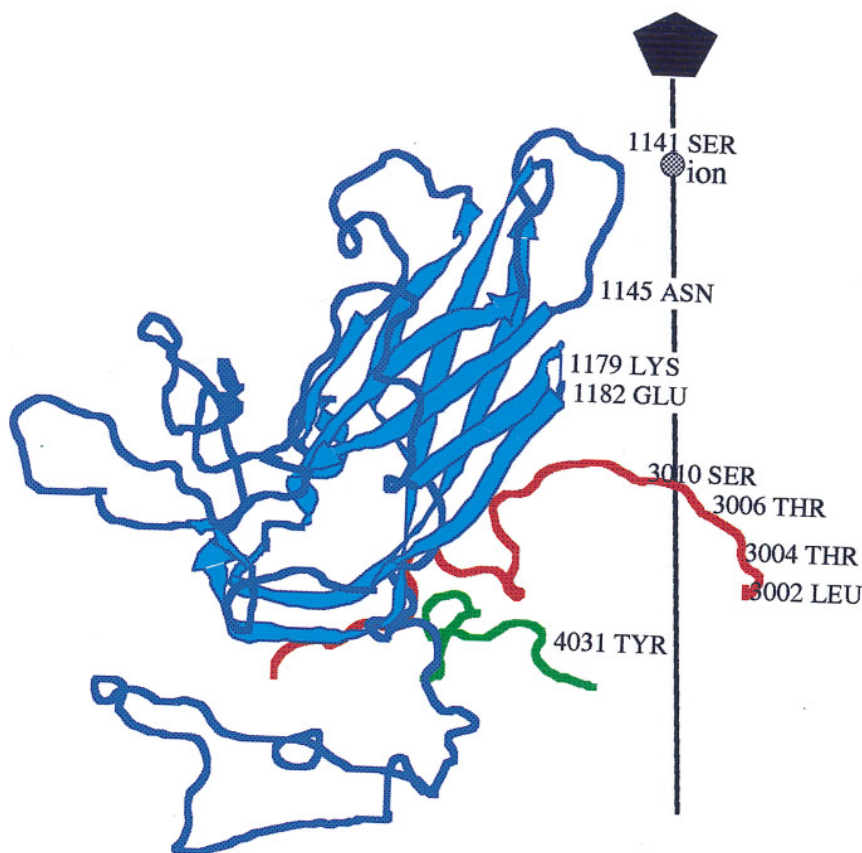


FIG. 5. Ribbon diagram of the protein structure surrounding the fivefold axis in HRV3 (blue, red, and green indicate VP1, VP3, and VP4, respectively). Labeled residues are closest to the fivefold axis.

fold axes (for HRV3, see Fig. 5) is very similar to that of  $\phi$ X174 (McKenna *et al.*, 1992; Ilag *et al.*, 1994) and coxsackievirus B3 (Muckelbauer *et al.*, 1995). Both viruses have a "vase-like" architecture surrounding the fivefold axes. Metal ions exist in the neck of both "vases" and most of the residues surrounding the fivefold axes are hydrophilic (Fig. 5). The DNA genome is ejected along a channel surrounding the fivefold axes of  $\phi$ X174 on infecting *Escherichia coli* (Yazaki, 1981). The similarities between rhinoviruses and  $\phi$ X174 in the structure of the protein surrounding the fivefold axes suggest the RNA genome of rhinoviruses might also be ejected along the fivefold axes. Evidence supporting this hypothesis is that when HRV14 crystals were exposed to acid vapor, HRV14 underwent conformational changes in the GH loop of VP1 and around the fivefold axis, with loss of  $\text{Ca}^{2+}$  on the fivefold axes (Giranda *et al.*, 1992).

While the capsid is required to be stable during transport between cells or between hosts, the virus must uncoat on entering the cell. The results reported here demonstrate that cation binding at fivefold axes in icosahedral viruses may be a fairly common mechanism to help regulate viral stability.

## ACKNOWLEDGMENTS

We are grateful to many members of our laboratory and to the CHES staff in helping with the data collection. We thank Bernd Berger, Marcos Oliveira and Bill Farrar for useful discussions and helping with the preparation of the EGTA-treated crystals. We thank Cheryl Towell and Sharon Wilder for help in the preparation of the manuscript. The work was funded by grants to MGR from the National Institute of Health and the former Sterling Winthrop Pharmaceutical Research Division. A Lucille P. Markey Foundation Award to MGR provided additional facilities for the structural biology faculty at Purdue University.

## REFERENCES

- Abdel-Meguid, S. S., Yamane, T., Fukuyama, K., and Rossmann, M. G. (1981). The location of calcium ions in southern bean mosaic virus. *Virology* **114**, 81–85.
- Aikens, D. A., and Reilley, C. N. (1963). Formation constants of metal complexes. In "Handbook of Analytical Chemistry" (L. Meites, Ed.), pp. 1–45. McGraw-Hill, New York.
- Brown, E. A., and Bugg, C. E. (1980). Calcium-binding to nucleotides: Structure of a hydrated calcium salt of inosine 5'-monophosphate. *Acta Crystallogr.* **B36**, 2597–2604.
- Brown, I. D., and Altermatt, D. (1985). Bond-valence parameters obtained from a systematic analysis of the inorganic crystal structure database. *Acta Crystallogr.* **B41**, 244–247.

- Brown, I. D., and Wu, K. K. (1976). Empirical parameters for calculating cation-oxygen bond valences. *Acta Crystallogr.* **B32**, 1957–1959.
- Concha, N. O., Head, J. F., Kaetzel, M. A., Dedman, J. R., and Seaton, B. A. (1993). Rat annexin V crystal structure: Ca<sup>2+</sup>-induced conformational changes. *Science* **261**, 1321–1324.
- DeSana, J., and Mandell, B. (1977). Studies on the in vitro uncoating of poliovirus. II. Characterization of the membrane-modified particle. *Virology* **78**, 554–566.
- Durham, A. C. H. (1977). Durham replies. *Nature (London)* **271**, 187.
- Durham, A. C. H. (1978). Cation binding and structural changes involved in plant virus disassembly. *Hoppe-Seyler's Z. Physiol. Chem.* **359**, 1047–1050.
- Filman, D. J., Syed, R., Chow, M., Macadam, A. J., Minor, P. D., and Hogle, J. M. (1989). Structural factors that control conformational transitions and serotype specificity in type 3 poliovirus. *EMBO J.* **8**, 1567–1579.
- Giranda, V. L., Heinz, B. A., Oliveira, M. A., Minor, I., Kim, K. H., Kolatkar, P. R., Rossmann, M. G., and Rueckert, R. R. (1992). Acid-induced structural changes in human rhinovirus 14: possible role in uncoating. *Proc. Natl. Acad. Sci. USA* **89**, 10213–10217.
- Glusker, J. P. (1991). Structural aspects of metal liganding to functional groups in proteins. *Adv. Prot. Chem.* **42**, 1–76.
- Greve, J. M., Davis, G., Meyer, A. M., Forte, C. P., Yost, S. C., Marlor, C. W., Kamarck, M. E., and McClelland, A. (1989). The major human rhinovirus receptor is ICAM-1. *Cell* **56**, 839–847.
- Hadfield, A. T., Lee, W.-M., Zhao, R., Oliveira, M. A., Minor, I., Rueckert, R. R., and Rossmann, M. G. (1997). The refined structure of human rhinovirus 16 at 2-15 Å resolution. *Structure*, submitted for publication.
- Hofer, F., Gruenberger, M., Kowalski, H., Machat, H., Huettinger, M., Kuechler, E., and Blaas, D. (1994). Members of the low density lipoprotein receptor family mediate cell entry of a minor-group common cold virus. *Proc. Natl. Acad. Sci. USA* **91**, 1839–1842.
- Hogle, J., Kirchhausen, T., and Harrison, S. C. (1983). Divalent cation sites in tomato bushy stunt virus. Difference maps at 2.9 Å resolution. *J. Mol. Biol.* **171**, 95–100.
- Hogle, J. M., Chow, M., and Filman, D. J. (1985). Three-dimensional structure of poliovirus at 2.9 Å resolution. *Science* **229**, 1358–1365.
- Ilag, L. L., McKenna, R., Yadav, M. P., BeMiller, J. N., Incardona, N. L., and Rossmann, M. G. (1994). Calcium ion-induced structural changes in bacteriophage  $\phi$ X174. *J. Mol. Biol.* **244**, 291–300.
- Jones, T. A., Zou, J.-Y., Cowan, S. W., and Kjeldgaard, M. (1991). Improved methods for building protein models in electron density maps and the location of errors in these models. *Acta Crystallogr.* **A47**, 110–119.
- Kim, S. (1989). Auto-indexing oscillation photographs. *J. Appl. Crystallogr.* **22**, 53–60.
- Kim, S., Smith, T. J., Chapman, M. S., Rossmann, M. G., Pevear, D. C., Dutko, F. J., Felock, P. J., Diana, G. D., and McKinlay, M. A. (1989). The crystal structure of human rhinovirus serotype 1A (HRV1A). *J. Mol. Biol.* **210**, 91–111.
- Lonberg-Holm, K., and Korant, B. D. (1972). Early interaction of rhinoviruses with host cells. *J. Virol.* **9**, 29–40.
- McKenna, R., Xia, D., Willingmann, P., Ilag, L. L., Krishnaswamy, S., Rossmann, M. G., Olson, N. H., Baker, T. S., and Incardona, N. L. (1992). Atomic structure of single-stranded DNA bacteriophage  $\phi$ X174 and its functional implications. *Nature (London)* **355**, 137–143.
- McPhalen, C. A., Strynadka, N. C. J., and James, M. N. G. (1991). Calcium-binding sites in proteins: a structural perspective. *Adv. Prot. Chem.* **42**, 77–144.
- Montelius, I., Liljas, L., and Unge, T. (1990). Sequential removal of Ca<sup>2+</sup> from satellite tobacco necrosis virus: structure of two EDTA-treated forms. *J. Mol. Biol.* **212**, 331–343.
- Muckelbauer, J. K., Kremer, M., Minor, I., Diana, G., Dutko, F. J., Groarke, J., Pevear, D. C., and Rossmann, M. G. (1995). The structure of coxsackievirus B3 at 3.5 Å resolution. *Structure* **3**, 653–667.
- Nayal, M., and Di Cera, E. (1994). Predicting Ca<sup>2+</sup>-binding sites in proteins. *Proc. Natl. Acad. Sci. USA* **91**, 817–821.
- Oliveira, M. A., Zhao, R., Lee, W. M., Kremer, M. J., Minor, I., Rueckert, R. R., Diana, G. D., Pevear, D. C., Dutko, F. J., McKinlay, M. A., and Rossmann, M. G. (1993). The structure of human rhinovirus 16. *Structure* **1**, 51–68.
- Pattanayek, R., Elrod, M., and Stubbs, G. (1992). Characterization of a putative calcium-binding site in tobacco mosaic virus. *Proteins* **12**, 128–132.
- Robinson, I. K., and Harrison, S. C. (1982). Structure of the expanded state of tomato bushy stunt virus. *Nature (London)* **297**, 563–568.
- Rossmann, M. G. (1979). Processing oscillation diffraction data for very large unit cells with an automatic convolution technique and profile fitting. *J. Appl. Crystallogr.* **12**, 225–238.
- Rossmann, M. G., Arnold, E., Erickson, J. W., Frankenberger, E. A., Griffith, J. P., Hecht, H. J., Johnson, J. E., Kamer, G., Luo, M., Mosser, A. G., Rueckert, R. R., Sherry, B., and Vriend, G. (1985). Structure of a human common cold virus and functional relationship to other picornaviruses. *Nature (London)* **317**, 145–153.
- Rossmann, M. G., Leslie, A. G. W., Abdel-Meguid, S. S., and Tsukihara, T. (1979). Processing and post-refinement of oscillation camera data. *J. Appl. Crystallogr.* **12**, 570–581.
- Rossmann, M. G., McKenna, R., Tong, L., Xia, D., Dai, J., Wu, H., Choi, H. K., and Lynch, R. E. (1992). Molecular replacement real-space averaging. *J. Appl. Crystallogr.* **25**, 166–180.
- Smith, T. J., Kremer, M. J., Luo, M., Vriend, G., Arnold, E., Kamer, G., Rossmann, M. G., McKinlay, M. A., Diana, G. D., and Otto, M. J. (1986). The site of attachment in human rhinovirus 14 for antiviral agents that inhibit uncoating. *Science* **233**, 1286–1293.
- Staunton, D. E., Merluzzi, V. J., Rothlein, R., Barton, R., Marling, S. D., and Springer, T. A. (1989). A cell adhesion molecule, ICAM-1, is the major surface receptor for rhinoviruses. *Cell* **56**, 849–853.
- Uncapher, C. R., DeWitt, C. M., and Colonno, R. J. (1991). The major and minor group receptor families contain all but one human rhinovirus serotype. *Virology* **180**, 814–817.
- Vedani, A., and Huhta, D. W. (1990). A new force field for modeling metalloproteins. *J. Amer. Chem. Soc.* **112**, 4759–4767.
- Yazaki, K. (1981). Electron microscopic studies of bacteriophage  $\phi$ X174 intact and 'eclipsing' particles, and the genome by the staining and shadowing method. *J. Virol. Methods* **2**, 159–167.
- Zhao, R., Pevear, D. C., Kremer, M. J., Giranda, V. L., Kofron, J., Rossmann, M. G., and Kuhn, R. J. (1996). The structure of human rhinovirus 3 at 3.0 Å resolution. *Structure*, **4**, 1205–1220.